Available online at www.sciencedirect.com
ScienceDirect
C. R. Geoscience 341 (2009) 517–525
COMPTES RENDUS GEOSCIENCE

Geomaterials (Ore deposits)

Ni-Co sulphide segregation in the Mamb pyroxenite intrusion, Cameroon

Charles Nkoumbou [a,*,b], Frédéric Villiéras [b], Pierre Barbey [c], Clément-Yonta Ngoune [a], Robert Joussemet [b], Frédéric Diot [b], Daniel Njopwouo [d], Jacques Yvon [b]

[a] *Équipe géologie économique et environnementale, département des sciences de la terre, faculté des sciences, université de Yaoundé I, BP 812, Yaoundé, Cameroun*
[b] *LEM, université de Nancy, CNRS, BP 40, 54501 Vandoeuvre-lès-Nancy cedex, France*
[c] *CRPG, université de Nancy, CNRS, BP 20, 54501 Vandoeuvre-lès-Nancy cedex, France*
[d] *Département de chimie inorganique, faculté des sciences, université de Yaoundé I, BP 812, Yaoundé, Cameroun*

Received 12 February 2008; accepted after revision 30 June 2009
Available online 8 August 2009

Presented by Zdenek Johan

Abstract

The amphibole metapyroxenite intrusion from Mamb (Cameroon) consists of enstatite, diopside-augite, edenite, and traces of plagioclase, biotite and rutile. It contains notable amounts of sulphides (pyrrhotite, pentlandite, chalcopyrite, pyrite and Co-rich violarite). The sulphide phase segregated during magma crystallization as immiscible droplets ($\leq$ 1 mm) included in growing ferromagnesian minerals or aggregated in the silicate crystal mush to form an interstitial phase. However, observed sulphide assemblages are likely to result from low-T ($\leq$ 300 °C) re-equilibration of high-T monosulphide solid solutions, more particularly during the Pan-African metamorphic event. The Mamb amphibole pyroxenite intrusion is tentatively considered as a potential source for Ni and Co mineralization. ***To cite this article: C. Nkoumbou et al., C. R. Geoscience 341 (2009).***

Résumé

Ségrégation de sulfures de Ni-Co dans l'intrusion de pyroxénite de Mamb, Cameroun. L'intrusion de métapyroxénite à amphibole de Mamb est constituée d'enstatite, diopside, édenite et de traces de plagioclase, biotite et rutile. Elle contient une quantité notable de sulfures tels que pyrrhotite, pentlandite, chalcopyrite, pyrite et violarite cobaltifère. Leur ségrégation s'est vraisemblablement produite à partir d'un magma silicaté. Au cours du refroidissement, des gouttelettes de sulfures ont été incluses dans les minéraux ferromagnésiens, ou se sont agrégées pour former une phase interstitielle. Cependant, les assemblages observés résultent du rééquilibrage des solutions solides initiales dans des conditions subsolidus de basse température ($\leq$ 300 °C), en liaison notamment avec le métamorphisme panafricain. Cette intrusion peut être considérée comme une source potentielle de minéralisations de Ni et Co. ***Pour citer cet article : C. Nkoumbou et al., C. R. Geoscience 341 (2009).***

Keywords: Pyroxenite; Sulphide; Ni-Co mineralization; Cameroon

Mots clés : Pyroxénite ; Sulfure ; Minéralisation à Ni-Co ; Cameroun

* Corresponding author.
E-mail address: nkoumbouc@yahoo.fr (C. Nkoumbou).

1631-0713/$ – see front matter
doi:10.1016/j.crte.2009.06.009

1. Introduction

In Cameroon, only one Ni-Co deposit is known as yet in the lateritic cover of serpentinites at Lomié (Fig. 1) [27,39]. Nevertheless, at the southern edge of the Pan-African belt (Mamb area; Fig. 1), the metamorphosed amphibole pyroxenite intrusion also contains Ni-Co sulphides. Owing to the economic Ni-Co-Cu potential linked to magmatic mafic-ultramafic rocks (e.g. Bushveld [21]; Kabanga in Tanzania [8]; Hongqiling in China [38]), the study of these sulphides is very attractive as they can be a window towards valuable indices. This article:

- presents a summary of petrogeochemical data;
- provides textural and mineralogical data on sulphides;
- discusses their magmatic segregation and subsequent subsolidus re-equilibration.

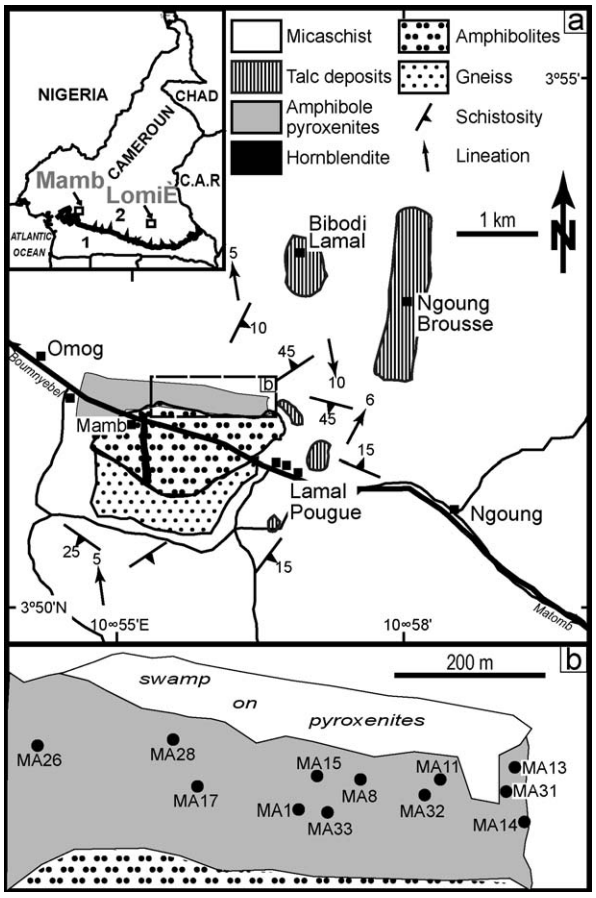

Fig. 1. **a:** geological sketch map of Mamb area showing the location of amphibole metapyroxenite; **b**: sample location. Insert: 1 = Congo craton, 2 = Pan-African thrust belt.

Fig. 1. **a** : carte géologique de la région de Mamb et localisation de la métapyroxénite à amphibole ; **b** : localisation des échantillons. Encart : 1 = Craton du Congo, 2 = Chaîne panafricaine charriée sur le craton.

2. Petrography and mineralogy of the amphibole pyroxenite

The southern domain of the Pan-African fold belt in Cameroon (Yaoundé group) consists of migmatitic gneisses partly covered by lower grade micaschist. To the east, the micaschist are associated with serpentinites and tholeiitic gabbro, whereas to the west, they are associated with amphibolite and talcschist [29,30]. At Mamb, an amphibole metapyroxenite occurs as metric boulders and flagstones in the forest, spread over $\approx 1000 \times 500$ m, and covered by 2–5 cm thick alteration products and purplish red soil. It is associated to a metagabbro intrusion dated at 618 ± 7 Ma [34], but no contact has been observed.

The rock is made up of orthopyroxene and clinopyroxene associated with abundant amphibole, occasional plagioclase and minute biotite flakes rimming amphibole grains (Table 1). The metapyroxenite is coarse-grained (Fig. 2) and porphyritic in the centre of the intrusion (most amphibole crystals ~ 2 cm), with well-preserved magmatic textures; whereas it is medium-grained towards the border. It is heterogeneous, with domains corresponding mainly to adcumulate or heteradcumulate, and locally to orthocumulate. There is no evidence of layering in the samples from the core, but the borders show a faint foliation. In adcumulate, subhedral pyroxene crystals form triple joints with no interstitial phase. In orthocumulate, interstitial minerals consist of sulphides, or plagioclase and amphibole, or plagioclase alone. Heteradcumulates are composed of cm-sized poikilitic hornblende megacrysts enclosing euhedral ortho- and clinopyroxene, anthophyllite and sulphide grains (Fig. 2a and b). Tiny Cr-spinel exsolutions ($Cr_2O_3 = 30$ wt.%) and high Al^{VI}/Al^{IV} ratios (≤ 2.6) in pyroxenes are typical of crystallization at high P conditions [36]. Thermobarometric estimates [15,28] yield pressures ranging from 2 to about 0.3 GPa, and crystallization temperature in the 1000–1350 °C and 650–1100 °C ranges for clino- and orthopyroxene, respectively. Plagioclase (< 5 vol.%) shows low anorthite content compared with most tholeiitic pyroxenites (An_{42-55} *vs.* An_{70-90} [3]). This may be related to plagioclase occurrence as a late interstitial phase after the crystallization of abundant diopside and Ca-amphibole, or to subsequent metamorphic re-equilibration. The poikilitic amphibole shows minute rutile exsolutions located along the cleavages, while the enclosed orthopyroxene is transformed into anthophyllite

Table 1
Composition and proportion of ferromagnesian phases in the metapyroxenite.
Tableau 1
Composition et proportion des phases ferromagnésiennes dans la métapyroxénite.

	vol.%	Composition	Mg#
Orthopyroxene	60–40	$Wo_{0-2}En_{65-75}Fs_{25-34}$	75–65
Clinopyroxene	30–25	$En_{40-45}Fs_{8-10}Wo_{45-50}$ and $En_{45-51}Fs_{11-14}Wo_{35-45}$	85–80
Edenite	20	$(Na_{0.31-0.35}K_{0.24-0.20})(Na_{0.21-0.17}Ca_{1.83-1.79})(Mg_{3.11-2.83}Fe^{3+}_{0.11-0.06}Fe^{2+}_{1.17-0.95}Mn_{0.01}Al^{VI}_{0.9-0.8})(Al^{IV}_{1.32-1.26}Ti_{0.22-0.16}Si_{6.53})O_{22}(OH)_2$	74–70
Mg-hornblende		$(Na_{0.28-0}K_{0.18-0.05})(Na_{0.41-0.07}Ca_{1.93-1.5})(Mg_{3.76-2.42}Fe^{3+}_{0.39-0}Fe^{2+}_{0.93-0.5}Mn_{0.02}Al^{VI}_{1.34-0.44})(Al^{IV}_{1.22-1.1}Ti_{0.17-0.06}Si_{7.31-6.58})$	82–70
Anthophyllite		$(Na_{0.06-0.04}K_{0.03-0.02})(Ca_{0.32-0.14}Mn_{0.04-0.02}Fe^{2+}_{0.96-0.79}Mg_{1.06-0.69})(Mg_{4.34-4.25}Cr_{0.05-0.03}Ti_{0.01}{}^{vi}Fe^{3+}_{0.70-0.62})({}^{iv}Fe^{3+}_{0.46-0.25}{}^{iv}Al_{0.52-0.40}Si_{7.23-7.14})$	73
Biotite	< 1	$(Mg_{4.25-3.41}Al_{1.2-0.5}Fe^{2+}_{1.43-1.0})(Si_{5.84-5.35}Al_{2.22-1.74})O_{20}(OH)_4(K_{1.81-1.53}Ba_{0.14-0.02}Na_{0.14-0.04}Ca_{0.14-0.01})$	81–70

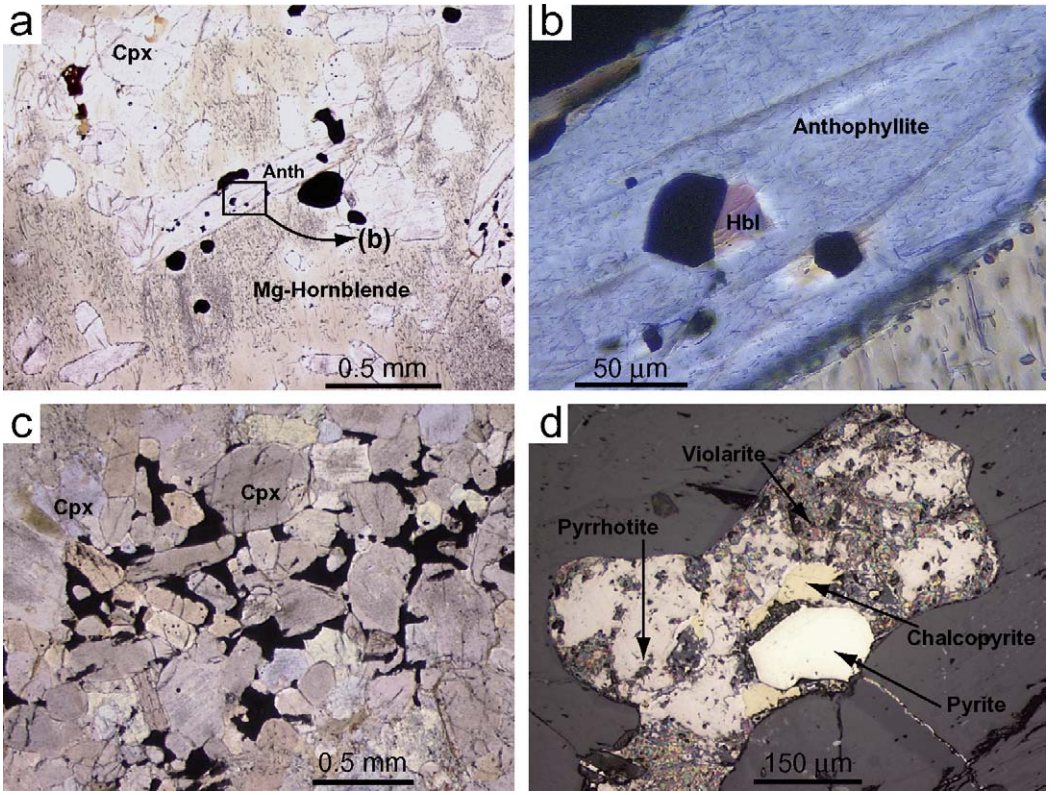

Fig. 2. Photomicrographs of sulphide microtextures. **a**: pyrrhotite inclusions in anthophyllite (Anth) in a poikilitic edenite of heteradcumulate (plane polarized light, PPL); **b**: enlargement of (**a**) showing euhedral sulphide inclusions, sometimes associated to hornblende in a sulphide-hornblende (Hbl) assemblage (PPL): **c**; interstitial sulphides (Cpx = diopside) (PPL); **d**: interstitial assemblage of pyrrhotite, chalcopyrite, pyrite and Co-rich violarite; note the patchy replacement of pyrrhotite by violarite (reflected light, RL).

Fig. 2. Microphotographies de textures des sulfures. **a** : inclusions de pyrrhotite dans une anthophyllite (Anth) englobée dans une édenite poecilitique d'un hétéradcumulat (LPNA) ; **b** : agrandissement montrant les inclusions de sulfures automorphes, parfois associées à la hornblende (Hbl) (LPA) ; **c** : sulfures interstitiels (LPNA) ; **d** : assemblage interstitiel de pyrrhotite, chalcopyrite, pyrite et violarite cobaltifère ; noter le remplacement de la pyrrhotite par la violarite (LR).

(Fig. 2a) suggesting some metamorphic re-equilibration. Other secondary transformations are occasional patches of anthophyllite in orthopyroxene, of hornblende in clinopyroxene and in primary edenite. Alteration also forms pockets along rare fissures, with talc replacing both amphibole and pyroxenes.

Chemically, the pyroxenite can be considered as an ultramafic subalkaline rock ($[Na_2O + K_2O] < 1.5$ wt.%,

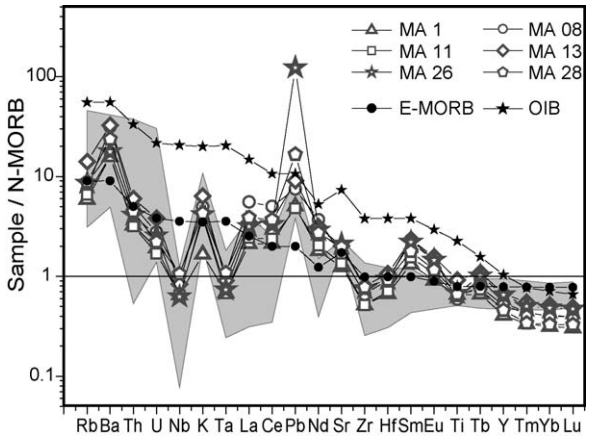

Fig. 3. N-MORB normalized multi-element diagram for Mamb pyroxenite samples compared to E-MORB, OIB and tholeiites from modern island-arcs (shaded field) [30,33]; note enrichment in selective large-ion lithophile elements along with Nb, Ta, Zr and Ti negative anomalies.

Fig. 3. Diagramme multiélémentaire normalisé au N-MORB pour des échantillons de pyroxénite de Mamb, comparés aux E-MORB, OIB et tholéïtes des arcs insulaires modernes (grisé) [30,33] ; noter l'enrichissement en certains éléments lithophiles et les anomalies négatives en Nb, Ta, Zr et Ti.

$K_2O < 0.5$ wt.% *vs* SiO_2 at 49 wt.%) akin to island arc tholeiite (Fig. 3). In the Dy/Yb *vs* La/Yb diagram (not shown), sample compositions plot above the experimental melting curve for garnet-bearing mantle. As cumulative pyroxenes cannot increase significantly the Dy/Yb ratio, the values of the studied samples might be indicative of higher proportion of garnet in the mantle source than in the referring experiment, considering the higher compatibility of Yb than Dy in garnet [2]. The high partial melting rates (20–25%) roughly deduced from this diagram are comparable to the values necessary for the generation of tholeiitic mafic-ultramafic melts [2,20]. On the whole, it appears that the parent magma likely originated from the mantle garnet stability field and dissolved high amounts of mantle sulphides.

3. Texture and chemistry of sulphide assemblages

Sulphide abundance decreases from the core of the massif (5 vol.%) towards its border (2 vol.%), roughly following the lithological evolution from porphyritic to granular pyroxenite. Sulphides consist in order of decreasing abundance of pyrrhotite, Co-rich violarite, chalcopyrite, pyrite and pentlandite. They show various occurrences.

Pyrrhotite (< 3 vol.%) occurs as euhedral rounded inclusions with size ≤ 100 µm in pyroxenes (Fig. 2a, b) and ≤ 1 mm in amphiboles. Some inclusions in amphibole consist of pyrrhotite, pentlandite, Co-rich violarite and chalcopyrite. Minute pyrrhotite inclusions in poikilitic amphibole display prismatic, oval or lamellar shapes, most lamellae occurring in the cleavage planes. As a whole, the distribution of these inclusions is very heterogeneous and does not feature the microtexture resulting from a necking-down process [1]. Sulphides with secondary amphibole in primary amphibole and pyroxene (Fig. 2a and b) can be attributed to the recrystallization of composite inclusions.

Sulphides (≤ 2 mm across) interstitial to pyroxene and amphibole comprise pyrrhotite, pentlandite, Co-violarite, chalcopyrite and secondary pyrite (Fig. 2c, d, and Fig. 4). Sulphide grains may be made up of distinct species. Violarite and chalcopyrite occur in pyrrhotite rimmed by secondary Ni-rich pyrite (Fig. 4a). There may also be aggregate of pyrrhotite, pentlandite, chalcopyrite, and patches of oxidised Ni-sulphide (Fig. 4c). Violarite and chalcopyrite form parallel lamellae with a crystallographic control in massive pyrrhotite. The sharp contact between violarite and pyrrhotite (Fig. 4b) supports a coherent exsolution [35] rather than a replacement origin. Similar characteristics were noted in hypogene violarite from Australia [10]. In other cases, occurrence as fringes along fractures and as well-developed replacement fronts inward grain margins of primary pyrrhotite testifies to a replacement origin (Fig. 2d). Such features are common in supergene zones of both massive and disseminated Ni deposits worldwide [10].

Mineral compositions were determined with an automated CAMECA SX100 electron microprobe (Université Henri-Poincaré, Nancy) and are available on request. Operating conditions for silicates and oxides were 15 kV acceleration voltage/20 nA probe current, and 20 kV/10 nA for sulphides, with counting time of 30 s for Au and Ag; 20 s for S, Fe, Co, Ni, Cu, Zn, As; 10 s for Ca, Ti, Mn, F, and 5 s for Na. Natural and synthetic oxides and metallic elements were used as standards, and the raw data were corrected using CAMECA X-PHI program. To avoid possible superficial oxidation of sulphides and particularly possible dissolution of sulphate [14], pure petroleum was used as polishing fluid. Scanning electron microscopy at 10 kV showed that there was no superficial oxidation. Because many experimental studies have found soluble oxygen in sulphide melts [e.g. 7, 24, 25, 37], most authors include oxygen among the elements in routine analysis of sulphide [11,18,37]. However, in the studied rocks, only altered sulphide crystals contain oxygen.

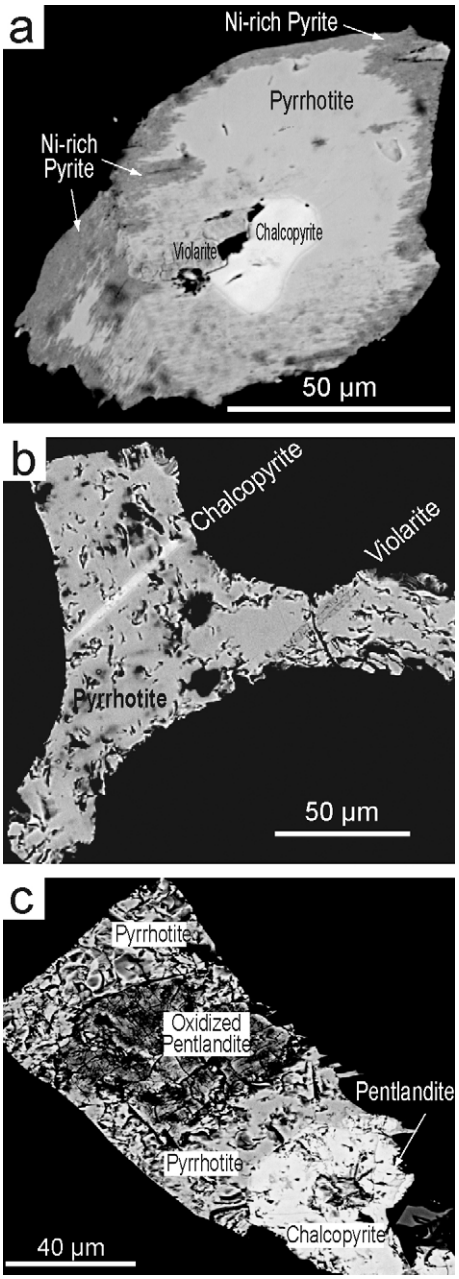

Fig. 4. Back-scattered photomicrographs of sulphide aggregates in pyrrhotite.

Fig. 4. Microphotographies en mode rétrodiffusé d'agrégats de sulfures dans la pyrrhotite.

Pyrrhotite corresponds to Ni-poor monosulphide ($Fe_{7.04-6.65}Ni_{0.055-0.024}S_8$), 5 wt.% Ni being the upper limit for pyrrhotite [11]. Compositions of pyrrhotite inclusions in orthopyroxene (42–45 at.% Fe) and those of inclusions in amphibole and interstitial assemblages (46 at.% Fe) correspond to monoclinic pyrrhotite [13]. Negative correlation between Fe and O contents ($R = -0.95$) with concomitant decrease in metal/anions ratio (M/S at.%) likely suggests metal leaching by fluids or during incipient alteration. Two analyses of inclusions in orthopyroxene contain notable amounts of Ni, Cu and Co (5.4, 4.5 and ∼1 at.%, respectively), which may be due to contamination by sub-microscopic exsolutions of a Ni-Co-Cu rich sulphide. Among minor elements, only Ag, Au and Bi were detected by the electron microprobe. Pyrrhotite inclusions in amphibole show the highest concentrations of Bi (≤ 0.34 wt.%).

Pentlandite occurs as exsolution in pyrrhotite inclusion within orthopyroxene contains 3.1 wt.% Co.

Chalcopyrite is the Cu-rich sulphide (Fig. 2f, 4c). All analyses are close to end-member compositions (M/S = 1.00 ± 0.05) despite some minor amounts of Co (< 0.25 wt.%) and Ni (< 0.25 wt.%) [11,19]. Oxygen contents are very low compared with those of the associated sulphides (0.10–0.24 *vs* 2.50–6.05 wt.%), showing that chalcopyrite is more resistant to alteration than pyrrhotite [19]. A few traces of Ag (0.11 wt.%) and Bi (0.21 wt.%) are noted.

Co-rich violarite composition is variable ($20 < Ni < 35$ and $8 < Co < 20$ wt.%). Traces of Au (0.4 ± 1.2 wt.%) and Ag (0.17 ± 0.23 wt.%) were detected but analytical uncertainties are too high for the contents to be significant. In Fig. 5a, the atomic Ni, Fe and Co contents normalized to 100% plot in the field of violarite with one trend towards Fe-rich (greigite) and the other towards Ni-rich components (linnaeite). High proportions of linnaeite component are found in the samples from the border while violarite from the core of the massif is close to ideal violarite ($FeNi_2S_4$). However, more detailed studies are necessary to establish the variations in composition and concentration of violarite in this intrusion, knowing that violarite is the most economically important member of the thiospinel group of minerals [10]. Negative correlation of Ni + Co to Fe (Fig. 5b) suggests the $2Fe \leftrightarrow Ni + Co$ substitution. They form a trend on the greigite–polydymite tie line, close to violarite *sl* (Fig. 6b). The M/S ratio values of violarite range from 0.60 to 0.70, taking into account the substitution of S by O, thus they display high metal deficit (0.3–0.4). There is a compositional gap between pyrrhotite and violarite (Fig. 5c), which suggests that the latter corresponds to secondary mineral formed mostly at the expense of pyrrhotite by either exsolution or dissolution-precipitation rather than by progressive conversion of pyrrhotite. High Co partitioning into violarite is a common feature in many base metal deposits.

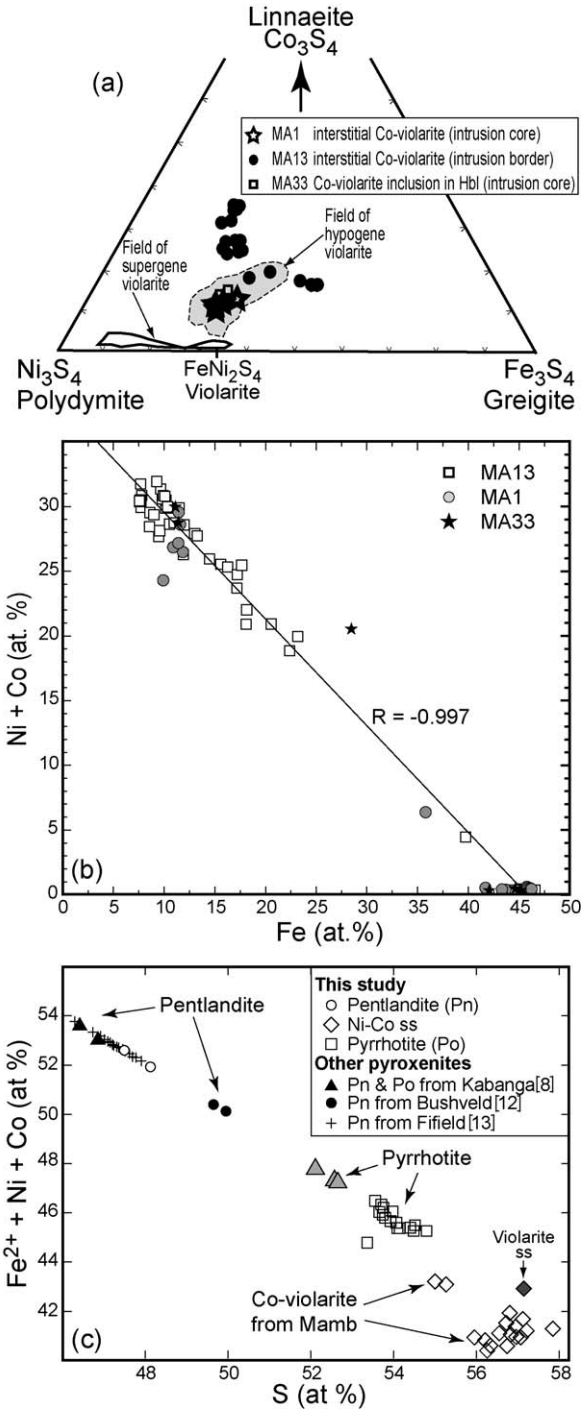

Fig. 5. Sulphide composition of the Mamb pyroxenite: **a** and **b**: compositions of Co-rich violarite in the Co_3S_4-Ni_3S_4-Fe_3S_4 ternary plot and in the Ni + Co vs. Fe diagram; **c**: Fe^{2+} + Ni + Co vs. S plot for Mamb sulphide minerals compared with other mineralized pyroxenites. Data set available on request.

Fig. 5. Composition des sulfures de la pyroxénite de Mamb : **a** and **b** : composition des violarites cobaltifères dans les diagrammes Co_3S_4-Ni_3S_4-Fe_3S_4 et Ni + Co-Fe ; **c** : diagramme Fe^{2+} + Ni + Co-S pour les sulfures de Mamb, comparés à ceux de pyroxénites minéralisées. Analyses disponibles sur demande.

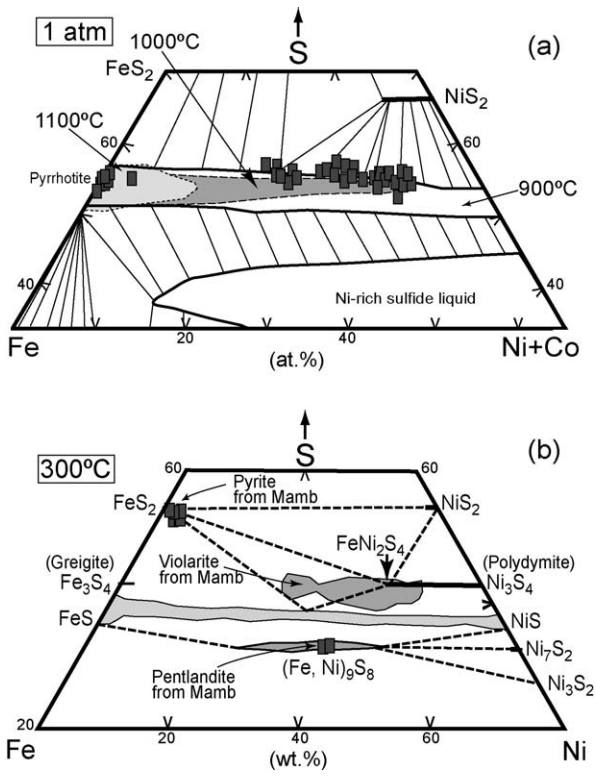

Fig. 6. **a**: Co-rich violarite compositions (at %) in the Fe-Ni-S system (mss stability fields at 1100, 1000 and 900 °C after [6]); **b**: pentlandite and Co-rich violarite compositions in the Fe-Ni-S system after [5].

Fig. 6. **a** : compositions des violarites cobaltifères dans le système Fe-Ni-S (domaines de stabilité à 1100, 1000 et 900 °C d'après [6]) ; **b** : composition de la pentlandite et des violarites cobaltifères dans le système Fe-Ni-S d'après [5].

Primary pyrite crystals (Fig. 2d) contain small amounts of Co (1.75–0.56 wt.%), with low Ni (< 0.06 wt.%), whereas secondary pyrite occurring as pseudomorph of pyrrhotite (Fig. 4a) shows notable amounts of Ni (6.12–5.50 wt.%), a feature common in pyrite from base metal sulphide deposits.

Most tholeiitic pyroxenites worldwide contain trace amounts of sulphides (< 1 vol.%) that consist of assemblages of pyrrhotite, chalcopyrite, occasional pentlandite and pyrite. Similar assemblages are also found in most base metal sulphide ore deposits from magmatic origin [3,8,12,13,20,22,26]. In a recent review, Maier [20] reported on many small intrusions that contain high-grade reefs of sulphide ores. Mamb pentlandite has a restricted range of sulphur content, and both pentlandite and pyrrhotite have higher S

content compared to those from other mineralized intrusions (Fig. 5c).

4. Discussion

Sulphide segregation from silicate melt is commonly interpreted from experimental data in terms of sulphide/silicate melt immiscibility at high T (1355–1300 °C) [6,7,14,23,24], concomitantly with the crystallisation of clino- and orthopyroxene. As a result, sulphide droplets occur as inclusions within these silicates. As T decreases in cumulate rocks, droplets of liquid sulphide are collected, migrate downward and fill the interstitial spaces [6,9,26], sulphide and oxide minerals reaching 80 vol.% in massive ores [8].

Pyrrhotite grains form inclusion in orthopyroxene and hornblende; composite grains of pyrrhotite + pentlandite and of chalcopyrite + pyrite + violarite occur as isolated inclusions in anthophyllite and poikilitic hornblende. As these inclusions cannot be exsolution features owing to the incompatible nature of S in most silicates and oxides [16], and keeping in mind that pyroxene may have crystallized at T conditions (650–1350 °C), we deduce that these sulphide inclusions are initially magmatic phases. Measured and predicted equilibration T for mss and sulphide liquid range from 850 to 1180 °C, and crystallisation of pyrrhotite begins at 1191 °C at 1 atmospheric pressure [6,7,23]. Accounting for the increase of the upper stability of sulphide with P (7 °C $kbar^{-1}$ [16], the sulphides should have crystallized at 1212–1332 °C at 0.3–2 GPa. Therefore, a possible simultaneous crystallization of pyroxenes and pyrrhotite may have allowed the pyrrhotite crystals to be included in pyroxene. When we plot our data in the Fe-(Ni + Co)-S diagram (Fig. 6a), pyrrhotite lays in the field of crystallization of mss at 1100 °C, while violarite compositions plot on the S-rich side of the fields of mss + liquid at 900–1000 °C [4,17], suggesting they are not the assemblages formed at high temperature, and comforting their secondary origin deduced from the textures.

The Fe-oxide-free sulphide assemblage in Mamb is better interpreted as the result from subsolidus lost of oxygen to the host silicate rock during cooling [25] rather than a feature of high-P assemblage considering the low solubility of oxygen in sulphide melts at high P [7,25].

Experiments have shown that high-T base metal sulphides undergo subsolidus recrystallization at low T, even in quenching experiments [31]. In the Mamb pyroxenite, many features of sulphide inclusions are characteristic of subsolidus recrystallization. The euhedral sulphide inclusions in pyroxene and amphibole contrast with the rounded sulphide inclusions indicative of sulphide melt immiscibility at high T [1], this shape being usually preserved after crystallization. It is likely that primary entrapment features of the studied sulphides were lost by subsolidus recrystallization, simply because Mamb pyroxenite emplaced during the early stage of the Pan African orogeny and suffered metamorphic recrystallization. This may have triggered sulphide recrystallization which yielded the various shapes of pyrrhotite inclusions in poikilitic amphibole.

Interstitial sulphide assemblages may correspond to mixture of different immiscible sulphide droplets [23], which have also suffered subsequent rearrangements. In the studied rock, all interstitial sulphides display typical recrystallization features: aggregates, lamellar exsolutions, low-T phase assemblages (pyrrhotite + pentlandite + violarite + chalcopyrite < 400 °C). Re-equilibration at low T is also suggested by:

- the Cu-free nature of pyrrhotite indicative of re-equilibration below 200 °C [17,35];
- the occurrence of secondary Ni-rich pyrite replacing pyrrhotite and suggesting late stage transformations inducing a shift from metal-rich mss to S-rich compositions;
- the plot of pentlandite compositions on the trend of pentlandite at 300 °C [5].

Some consider that violarite corresponds to any intermediate composition between greigite and polydymite rather than just to the Ni_2FeS_4 composition [32]. Accordingly, the trend of violarite (Fig. 6b) and the high Ni and Co contents of Mamb phases could result from low-T re-equilibration (< 200 °C), similarly to hypogene violarite + pentlandite ± pyrite assemblages reported from Nickel sulphide ore body at Mount Keith, central Western Australia [10].

5. Conclusions

The Mamb amphibole metapyroxenite results from the crystallization of a primitive (Mg# = 75–71, Cr = 1503–1107 ppm), mantle-derived tholeiitic magma. It contains pentlandite, pyrrhotite, Co-rich violarite, chalcopyrite and pyrite. Compositions of Co-rich violarite vary significantly, whereas those of other sulphides are close to ideal compositions. Sulphide inclusions in clinopyroxene are best explained by sulphide segregation from silicate magma at high temperature and pressure. Cooling and sub-sequent

metamorphism led to successive re-equilibration of all sulphide assemblages down to 200 °C. The textures point to a possible sulphide sinking in the cumulative pile but massive ores are yet to be discovered. As the amphibole pyroxenite outcrops at a level land, geophysical survey and detailed mapping are needed to check whether this ultramafic body contains hidden sulphide-rich reefs and/or screen units of sulphides ore.

Acknowledgements

Stays of the first author at LEM-CNRS (Nancy, France) and analyses were granted by both ''Mission de coopération française au Cameroun'' and CNRS. The thorough review and suggestions by M. Ohnenstetter are gratefully acknowledged.

References

[1] T. Andersen, W.L. Griffin, S.Y. O'reilly, Primary sulphide melt inclusions in mantle-derived megacrysts and pyroxenites, Lithos 20 (1987) 279–294.
[2] P.J.F. Bogaard, G. Wörner, Petrogenesis of basanitic to tholeiitic volcanic rocks from the Miocene Vogelsberg, Central Germany, J. Petrol. 44 (2003) 569–602.
[3] R.G. Cawthorn, K. Boerst, Origin of pegmatitic pyroxenite in the Merensky unit, Bushveld complex, South Africa. J. Petrol. 47 (2006) 1509–1530.
[4] J.R. Craig, Pyrite-pentlandite assemblages in the Fe-Ni-S system, Am. J. Sci. 273A (1973) 496–510.
[5] J.R. Craig, G. Kullerud, Phase relations in the Cu-Fe-Ni-S system and their applications to magmatic ore deposits, Econ. Geol. Monogr. 4 (1969) 343–358.
[6] D.S. Ebel, A.J. Naldrett, Fractional crystallization of sulfide ore liquids at high temperature, Econ. Geol. 91 (1996) 607–621.
[7] D.S. Ebel, A.J. Naldrett, Crystallization of sulfide liquids and interpretation of ore composition, Can. J. Earth Sci. 34 (1997) 352–365.
[8] D.M. Evans, L. Byemelwa, J. Gilligan, Variability of magmatic sulphide compositions at the Kabanga nickel prospect, Tanzania, J. Afr. Earth Sci. 29 (1999) 329–351.
[9] B. Godel, S.-J. Barnes, W.D. Maier, Platinum-group elements in sulphide minerals, Platinum-group minerals, and whole-rocks of the Merensky Reef (Bushveld Complex, South Africa): Implications for the formation of the Reef, J. Petrol. 48 (2007) 1569–1604.
[10] B.A. Grguric, Hypogene violarite of exsolution origin from Mount Keith, Western Australia: field evidence for a stable pentlandite-violarite tie line, Min. Mag. 66 (2002) 313–326.
[11] J. Guo, W.L. Griffin, S.Y. O'reilly, Geochemistry and origin of sulphide minerals in mantle xenoliths: Qilin, southeastern China, J. Petrol. 40 (1999) 1125–1149.
[12] D.A. Howell, I. McDonald, Distribution of platinum-group elements in the Platreef at Overysel, northern Bushveld Complex: a combined PGM and LA-ICP-MS study, Contrib. Mineral. Petrol. 154 (2007) 171–190.
[13] Z. Johan, M. Ohnenstetter, E. Slansky, L.M. Barron, D. Suppel, Platinium mineralization in the Alaskan-type intrusive complexes near Fifield, New South Wales,Australia: Part 1. Platinium-group minerals in clinopyroxenites of the Kelvin prospect, Owendale Intrusion, Mineralogy and Petrology 40 (1989) 289–309.
[14] P.J. Jugo, R.W. Luth, J.P. Richards, An experimental study of the sulfur content in basaltic melts saturated with immiscible sulfide or sulfate liquids at 1300 °C and 1.0 Gpa, J. Petrol. 46 (2005) 783–798.
[15] D. Lindsley, Pyroxene thermometry, Am. Mineral. 68 (1983) 477–493.
[16] J.P. Lorand, The Cu-Fe-Ni sulphide component of the amphibole-rich veins fom the Lherz and Freychinède spinel peridotite massifs (northeastern Pyrenees, France): A comparison with mantle-derived megacrysts from alkali basalts, Lithos 23 (1989) 281–298.
[17] J.P. Lorand, M. Grégoire, Petrogenesis of base metal sulphide assemblages of some peridotites from the Kaapvaal craton (South Africa), Contrib, Mineral. Petrol. 151 (2006) 521–538.
[18] A. Luguet, J.P. Lorand, M. Seyler, Sulphide petrology and high siderophile element geochemistry of abyssal peridotites: A coupled study of samples from the Kane Fracture Zone (45°W 23°20N, MARK Area, Atlantic ocean), Geochim. Cosmochim. Acta 67 (2003) 1553–1570.
[19] N.D. Macfarlane, D.J. Mossman, The opaque minerals and economic geology of the Nemeiben utramafic complex, Saskatchewan, Canada, Mineral Deposita 16 (1981) 409–424.
[20] W.D. Maier, Platinium group elements (PGE) deposits and occurrences: Mineralization styles, genetic concepts, and exploration criteria, J. Afr. Earth Sci. 41 (2005) 165–191.
[21] R.K.W. Merkle, G. von Gruenewaldt, Compositional variation of Co-rich pentlandite: relation to the evolution of the Upper Zone of the western Bushveld complex, South Africa, Can. Mineral. 24 (1986) 529–546.
[22] A. Mogessie, Ch.A. Hauzenberger, G. Hoinkes, A. Felfernig, E.F. Stumpfl, E.A. Bjerg, J. Kostadinoff, Genesis of platinum-group minerals in the Las Aguilas mafic-ultramafic rocks, San Luis Province, Argentina: textural, chemical and mineralogical evidence, Mineralogy and Petrology 68 (2000) 85–114.
[23] J.E. Mungall, Crystallization of magmatic sulfides: an empirical model and application to Sudbury ores, Geochim. Cosmochim. Acta 71 (2007) 2809–2819.
[24] J.E. Mungall, S. Su, Interfacial tension between magmatic sulphide and silicate liquids: Constraints on kinetics of sulphide liquation and sulphide migration through silicate rocks, Earth Planet. Sci. Lett. 234 (2005) 135–149.
[25] A.J. Naldrett, A portion of the system Fe-S-O between 900 and 1080 °C and its application to sulfide ore magmas, J. Petrol. 10 (1969) 171–201.
[26] A.J. Naldrett, A.H. Wilson, Horizontal and vertical variations in noble-metal distribution in the Great Dyke of Zimbabwe: a model for the origin of the PGE mineralization by fractional segregation of sulfide, Chem. Geol. 88 (1990) 279–300.
[27] Z.H.P. Ndonguissop, C. Nkoumbou, M. Mbogning, B. Agbor, B. Bat, A.C. Seme Mouangue, E. Simo, B. Ayongaba, C. Omgba, Exploration of the Cobalt–Nickel bearing laterites of Nkamouna (Lomié region, South-East Cameroon), Geovic Technical report 4 (1999) (68 p + 300 pages of logs + maps in the annex).
[28] P. Nimis, P. Ulmer, Clinopyroxene geobarometry of magmatic rocks, Part 1. An expanded structural geobarometer for anhydrous and hydrous basic and ultrabasic systems, Contribution to Mineralogy and Petrology 133 (1998) 122–135.

[29] C. Nkoumbou, D. Njopwouo, F. Villiéras, A. Njoya, C. Yonta Ngouné, L. Ngo Ndjock, F. Tchoua, J. Yvon, Talc indices from Boumnyebel (Centre–Cameroon), physicochemical characteristics and geochemistry, J. Afr. Earth Sci. 45 (2006) 61–73.

[30] C. Nkoumbou, C. Yonta Ngouné, F. Villiéras, P. Barbey, D. Njopwouo, J. Yvon, Petrogenesis of Amphibole Pyroxenites from the Pan-African Yaoundé Group (Cameroon): Geodynamic implications, J. Afr. Earth Sci. submitted.

[31] A. Peregordova, M. Ohnenstetter, Collectors of Pt, Pd and Rh in a S-poor Fe-Ni-Cu sulphide system at 760 °C: experimental data and application to ore deposits, Cana. Mineral. 40 (2002) 527–561.

[32] A. Pring, C. Tenailleau, B. Etschmann, J. Brugger, B. Grguric, The transformation of pentlandite to violarite under hydrothermal conditions: a dissolution-reprecipitation reaction, in : I.C. Roach (Ed.), Regolith - Ten Years of CRC LEME, 2005, 252–255.

[33] S.-s. Sun, W.F. McDonough, Chemical and isotopic systematics of oceanic basalts: implications for mantle composition and processes. In: A.D. Saunders, M.J. Norry, (Eds.), Magmatism in the Ocean Basins, Geol. Soc. Spec. Pub. 42 (1989) 313–345.

[34] S.F. Toteu, R. Yongue Fouateu, J. Penaye, J. Tachakounté, A.C. Seme Mouangue, W.R. Van Schmus, E. Deloule, H. Stendal, U-Pb dating of plutonic rocks involved in the nappe tectonic in southern Cameroon: consequence for the Pan-African orogenic evolution of the central African fold belt, J. Afr. Earth Sci. 44 (2006) 479–493.

[35] D.J. Vaughan, J.R. Craig, Mineral chemistry of metal sulfides, Cambridge University Press, Cambridge, 1978 493 p.

[36] S. Wass, Multiple origins of clinopyroxenes in alkali basaltic rocks, Lithos 12 (1979) 115–132.

[37] R.F. Wendlandt, Sulfide saturation of basalt and andesite melts at high pressures and temperatures, Am. Mineral. 67 (1982) 877–885.

[38] F. Wu, S. Wilde, G. Zhang, D. Sun, Geochronology and petrogenesis of the post-orogenic Cu-Ni sulphide-bearing mafic-ultramafic complexes in Jilin Province, NE China, J. Asian Earth Sci. 23 (2004) 781–797.

[39] R. Yongue-Fouateu, R.T. Ghogomu, J. Penaye, G.E. Ekodeck, H. Stendal, F. Colin, Nickel and cobalt distribution in laterite from Lomié region, south-east Cameroon, J. Afr. Earth Sci. 45 (2006) 33–47.